



# Precipitation variability using GPCC data and its relationship with atmospheric teleconnections in Northeast Brazil

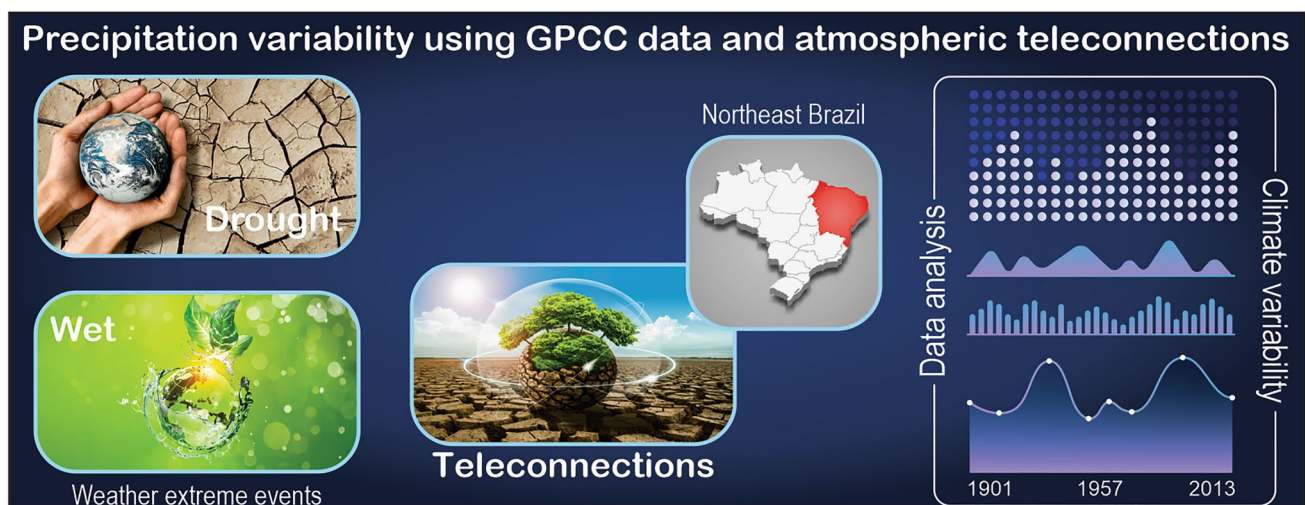
Daris Correia dos Santos<sup>1</sup> · Celso Augusto Guimarães Santos<sup>1</sup> · Reginaldo Moura Brasil Neto<sup>1</sup> ·  
Richarde Marques da Silva<sup>2</sup> · Carlos Antonio Costa dos Santos<sup>3</sup>

Received: 29 July 2022 / Accepted: 19 May 2023 / Published online: 4 June 2023  
© The Author(s) 2023

## Abstract

The present study investigates the influence of different atmospheric teleconnections on the annual precipitation variability in Northeast Brazil (NEB) based on the annual precipitation data from the Global Precipitation Climatology Center (GPCC) from 1901 to 2013. The objective of this study is to analyze the influence of different atmospheric teleconnections on the total annual precipitation of NEB for the 1901–2013 period, considering the physical characteristics of four subregions, i.e., Mid-north, Backwoods, Agreste, and Forest zone. To analyze the influence of different atmospheric teleconnections, GPCC data were used, and the behavior of the teleconnections was assessed using Pearson correlation coefficient, Rainfall Anomaly Index (RAI), and cross-wavelet analysis. The Pearson correlation was used to analyze the influence on the annual precipitation for the studied region. RAI was used to calculate the frequency of atmospheric patterns and drought episodes. The cross-wavelet analysis was applied to identify similarity signals between precipitation series and atmospheric teleconnections. The results of the Pearson correlation assessed according to Student's *t* test and cross-wavelet analysis showed that the Atlantic Multidecadal Oscillation (AMO) exerts a more significant influence on the Backwoods region at an interannual scale. In contrast, the Pacific Decadal Oscillation (PDO) exerts greater control over the modulation of the climatic patterns in NEB. The results of the study are insightful and reveal the differential impacts of teleconnections such as the AMO, PDO, MEI, and NAO on precipitation in the four sub-regions of NEB. The Atlantic circulation patterns strongly influence the interannual and interdecadal precipitation in the Agreste, Backwoods, and Mid-north regions, possibly associated with the Intertropical Convergence Zone (ITCZ) position. Finally, this study contributes to understanding internal climatic variability in NEB and planning of water resources and agricultural activities in such a region.

## Graphic abstract



Extended author information available on the last page of the article

**Keywords** Coherence wavelet · Drought · Oscillation · Teleconnections

## 1 Introduction

Atmospheric teleconnections serve as a bridge between different oceanic regions, facilitating the transfer of energy and influencing global climate dynamics (Zhou et al. 2022). They help restore imbalances in the climate system's energy budget, which result from the meridional distribution of solar insolation and sea surface temperature (SST) anomalies associated with the El Niño-Southern Oscillation (ENSO) and internal climate variability (Stan et al. 2017). These phenomena have motivated numerous observational studies, either on a global scale or focusing on specific regions, with some research demonstrating that teleconnections involve both oceanic and atmospheric fields (e.g., Grimm and Saboia 2015; Ndehedehe et al. 2018; Lim et al. 2018; Park and Li 2018).

A variety of studies have investigated the atmospheric patterns generated by SST variability in the Atlantic and Pacific Oceans, highlighting their important role in global climate dynamics on interannual and multidecadal temporal scales (Chiang and Friedman 2012; Lau 2015; Cabré et al. 2017). These patterns can evolve and be modulated by the interaction of different teleconnection processes on various time scales. The Pacific Decadal Oscillation (PDO) and Atlantic Multidecadal Oscillation (AMO) are the primary dominant modes on decadal and multidecadal scales, while the North Atlantic Oscillation (NAO) and Multivariate ENSO Index (MEI) contribute to regional internal climatic variability on an inter-annual scale (Vining et al. 2022). The modulation of the PDO and the NAO involves the interaction between tropical SSTs, which helps to better understand the interannual impacts of ENSO warm and cold events in relation to the PDO and AMO phases (Han et al. 2022).

Spatiotemporal variations of extreme precipitation regimes are both caused by climate change. Hence, understanding their characteristic scales in space and time is crucial to allocating and managing local water resources (Chang et al. 2018). Furthermore, understanding the role of climate variability in precipitation modulation is important for seasonal predictability and a better understanding of global climate fluctuations, resulting in an improved explanation of rainfall variability (Jemai et al. 2017). Climate variability and large-scale climate teleconnections strongly impact the regional climate and hydrological variability in many parts of the world (Xiao et al. 2016; Huo et al. 2016). Therefore, finding the association between meteorological elements and the oscillatory pattern of climatic teleconnections can be very helpful in improving the accuracy of hydro-meteorological predictions and help in the prediction of extreme

weather events, such as drought or floods, and also in the management of water resources (Araghi et al. 2016; Nascimento et al. 2022).

Precipitation in Northeast Brazil (NEB) presents high spatiotemporal variability and irregular rainfall (Brito et al. 2021; Silva et al. 2022). Overall, the irregular rainfall in NEB can have significant social, economic, and environmental impacts, and it is important to develop strategies to mitigate its effects and adapt to the changing climate. The main problems caused by irregular rainfall are drought, flooding, soil erosion, reduced availability of water, impacts on biodiversity, and health impacts. Regarding the relationship between rainfall and atmospheric teleconnections, according to Brahmananda Rao and de Brito (1985), during winter, the circulation characteristics over the North Atlantic Ocean seem to be related to the circulation characteristics of other regions in the Northern Hemisphere. This suggests that NEB rainfall may have interesting teleconnections with the circulation characteristics of other regions in the Northern Hemisphere.

Therefore, it is crucial to investigate the influence of atmospheric teleconnections on the precipitation pattern that may lead to the intensification of internal climatic variability or climatic changes (Silva et al. 2020). The population in such a region is vulnerable to the impacts of climate change primarily because of the socioeconomic and political context in which they live. According to Delazeri et al. (2022), climate change can exacerbate access to basic needs, making it harder for vulnerable populations to obtain these necessities. Climate change-induced events such as floods, droughts, and hurricanes can displace communities, forcing them to migrate to other regions. These migrations can lead to increased economic and social vulnerabilities, especially for those who are compelled to leave their homes without sufficient resources, resulting in instability and poverty (Da Silva et al. 2022). Moreover, the population and production in the region rely on rainfall events to sustain agricultural production and daily water consumption, as rainwater is captured in cisterns for storage (Dantas et al. 2020).

Mainly, this is because NEB is an agriculturally based developing region facing the challenge of feeding rapidly growing populations in the coming decades (Thornton et al. 2014). The performance of different meteorological systems and the deficiency of public policies in managing water resources or severe weather warnings favor the occurrence of economic losses and human lives in NEB (Silva et al. 2017). Understanding rainfall variability is essential for dealing with the scarcity of water resources due to increasing

water demand, population growth, and economic development (Surendran et al. 2019).

As a major aspect of the water circulation system, the spatiotemporal distribution of regional precipitation is inevitably affected by climatic factors, which may induce a series of hydrologic disasters, including drought and flood (Verdon et al. 2004; Dufek and Ambrizzi 2008; Kundzewicz et al. 2010; Leng et al. 2015), and extreme precipitation events that are among the most disruptive of atmospheric phenomena (Zin et al. 2010). To analyze these events, well-distributed and consistent data with the ability to capture the rainfall regime in the planet's most remote and poorly instrumented regions are needed. Nowadays, the Global Precipitation Climatology Centre (GPCC) (Schamm et al. 2014) provides gridded gauge-analysis products derived from quality controlled station data, which are adequate for analysis of the effect of atmospheric teleconnections on rainfall variability. Several studies have used the time series of GPCC to investigate the evolution of atmospheric teleconnections in precipitation (e.g., Molavi-Arabshahi et al. 2015; Okumura et al. 2017; Wang et al. 2018), and the results are satisfactory.

It is important to note that many studies have used advanced statistical analysis, such as wavelet (Santos et al.

2019, 2023; Alizamir et al. 2023) to detect statistically significant interannual and interdecadal oscillations in the patterns of precipitation variability and atmospheric teleconnections (e.g., Chang et al. 2018; Santos et al. 2018, 2013; Su et al. 2017; Jemai et al. 2017) and this tool has been shown to be very useful for this purpose (Zhao et al. 2022; Fan et al. 2022).

Brahmananda Rao and de Brito (1985) analyzed teleconnections between the rainfall over NEB and the Winter Circulation of Northern Hemisphere. Teleconnections are noted to be stronger during the winter season, and interannual variations of rainfall over NEB are associated with variations in the Northern Hemisphere winter circulation. Recently, Costa et al. (2018) showed that global climate oscillations have a non-stationary relationship with the NEB rainy season, impacting the hydrology of the study area at different time scales. In this sense, given the spatiotemporal variability of precipitation over NEB, the objective of this study is to evaluate the influence of different atmospheric teleconnections on the total annual precipitation of NEB for the 1901–2013 period, considering the physical characteristics of four subregions, i.e., Mid-north, Backwoods, Agreste, and Forest zone.

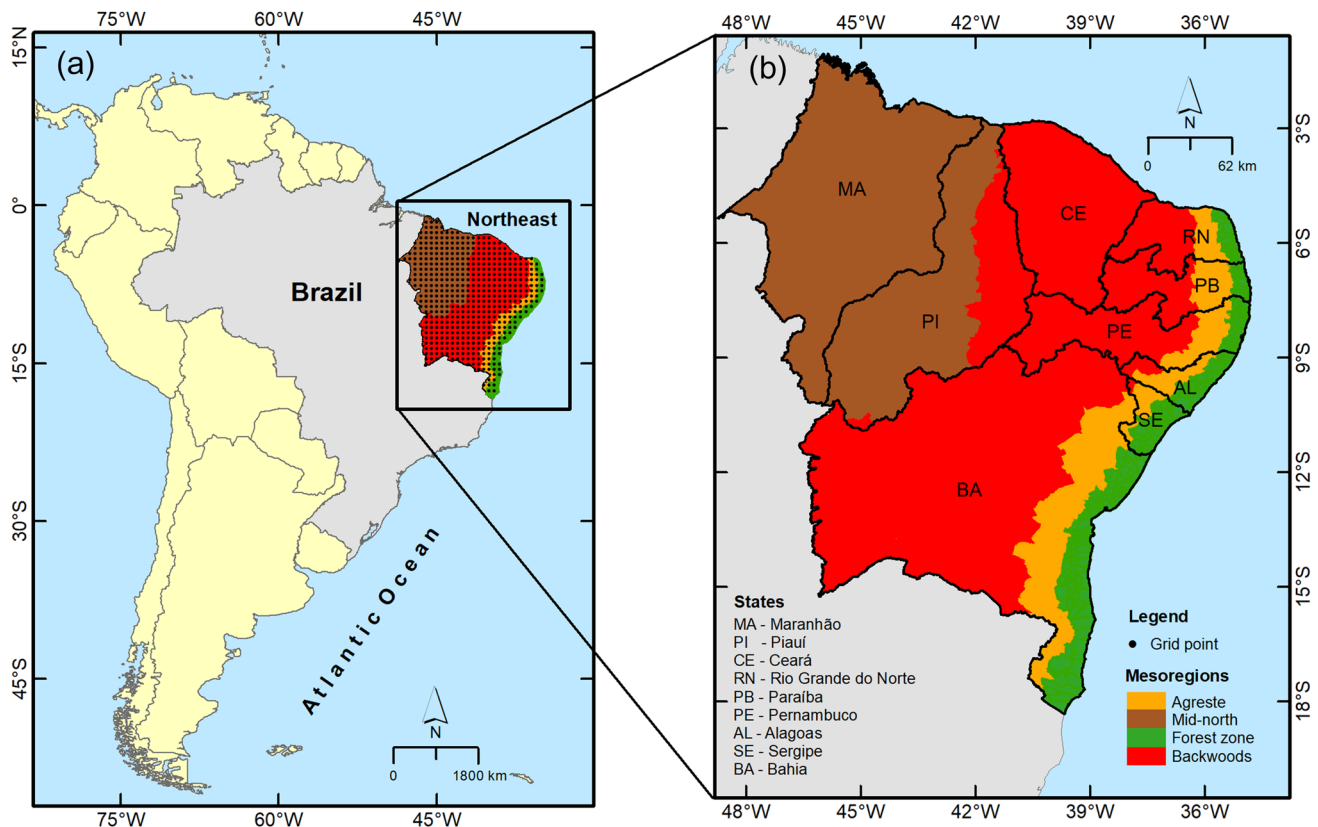


Fig. 1 HYPERLINK "sps:did:fig1lllocator::gr1llMediaObject::0" Location of Northeast Brazil and mesoregions

## 2 Data and methodology

### 2.1 Study area

The study region, located between the parallels 01°02'30"N and 18°20'07"S and between the meridians 34°47'30"W and 48°45'24"W (Fig. 1), encompasses the states of Alagoas, Bahia, Ceará, Maranhão, Paraíba, Piauí, Pernambuco, Rio Grande do Norte, and Sergipe. These states account for a total area of 1,561,177 km<sup>2</sup>, representing 18.26% of Brazil's total area, with a population density of 30.54 inhab./km<sup>2</sup>. The study area's delimitation concentrates around 89.5% of Brazil's semiarid region, covering most of the states in the region except for Maranhão (IBGE 2010). This study analyzed precipitation variability using GPCC data and its relationship with atmospheric teleconnections in NEB, employing the division proposed by Andrade (1980), which divided NEB into four physiographic mesoregions: Mid-north (Meio-Norte), Forest zone (Zona da Mata), Agreste, and Backwoods (Sertão). The criteria used to define the four sub-regions in NEB are climate, vegetation, presence of mountains, and geographical location. These factors help us understand the specific characteristics of each sub-region, such as their unique strengths and challenges. By considering these criteria, policymakers and regional planners can develop targeted strategies to promote sustainable development and improve the overall well-being of the region's inhabitants (Moreira et al. 2007). Thus, each subdivision analyzed has distinct physical characteristics and precipitation regimes.

The Forest zone is a coastal region with a humid tropical climate, featuring well-distributed rainfall throughout the year and coastal mountains and plateaus. The predominant vegetation is the Atlantic Forest, with extensive production of sugarcane. The Agreste is a region with the presence of

mountains and plateaus, has a mild climate, and the predominant vegetation is a transition between the Atlantic Forest and the Caatinga. This region is a transition zone between the Forest zone and the Backwoods. The Forest zone is located in the east and has the highest precipitation values in NEB (Brasil Neto et al. 2020).

The Backwoods is a region with the presence of mountains and plateaus, a hot and dry climate, with irregular and concentrated rainfall in a few months of the year, typical of the semiarid climate. This subregion presents irregular and scarce rainfall, besides periods of drought, and its typical vegetation is the Caatinga and Savannah (Silva et al. 2018). The Mid-north is a more northern region, composed of Maranhão and Piauí. It has a hot and humid climate, with the presence of Cerrado and Caatinga. In the Mid-north, precipitation varies from 2000 to 1500 mm/year.

The predominant climates in NEB are the humid equatorial climate that covers a small part of the state of Maranhão and the border of the state of Pará (Silva Junior et al. 2020); the humid coastal climate that covers the coast from the states of Bahia to the Rio Grande do Norte; a tropical climate that predominates in the states of Bahia, Ceará, Maranhão, and Piauí; and the semiarid tropical climate that occurs in most of the NEB states, except for Maranhão (Safanelli et al. 2023).

NEB is also characterized by irregular rains and prolonged drought occurrences that affect the main economic activities in the agricultural sector and livestock (Brasil Neto et al. 2022). The region's geographical position, relief, and pressure systems are among the main climatic factors determining the distribution of climatic elements in NEB and the seasonal variation (Kayano and Andreoli 2009). Among the large-scale phenomena that act over NEB, the Intertropical Convergence Zone and El Niño-Southern Oscillation are the most important (Hastenrath and Lamb 1977; Chiang et al. 2002; Giannini et al. 2004).

**Table 1** Indices, abbreviations, and descriptions of the teleconnections analyzed

Index	Abbreviation	Description
Atlantic Multidecadal Oscillation	AMO	The AMO has been identified as a coherent mode of natural variability occurring in the North Atlantic Ocean with an estimated period of 60–80 years (NCAR 2019)
Pacific Decadal Oscillation	PDO	The PDO is a pattern of Pacific climate variability similar to ENSO in character but varies over a much longer time scale and can remain in the same phase for 20 to 30 years, while ENSO cycles typically only last 6 to 18 months (NCSU 2019)
North Atlantic Oscillation	NAO	The NAO index is based on the surface sea-level pressure difference between the Subtropical (Azores) High and the Subpolar Low. The positive phase of the NAO reflects below-normal heights and pressure across the high latitudes of the North Atlantic and above-normal heights and pressure over the central North Atlantic, the eastern United States, and western Europe. The negative phase reflects an opposite pattern of height and pressure anomalies over these regions (NCDC 2019)
Multivariate ENSO Index	MEI	Weighted anomaly average of six meteorological variables in the tropical Pacific: sea surface temperature, sea level pressure, surface air temperature, components of surface wind zonal and meridional, and component total cloudiness fraction of the sky (NCAR 2019)

## 2.2 Dataset used

The data series used in this research is based on monthly precipitation data from the GPCC for the 1901–2013 period (available data), with  $0.5^\circ \times 0.5^\circ$ ,  $1.0^\circ \times 1.0^\circ$ , and  $2.5^\circ \times 2.5^\circ$  spatial resolutions (Schneider et al. 2016). In this study, we used the GPCC 7.0 product with a  $0.5^\circ \times 0.5^\circ$  spatial resolution. GPCC provides global monthly rainfall estimates, which are solely based on ground observations from around 75,100 stations worldwide that feature at least 10 years of records (Basheer and Elagib 2016). These data were used to estimate the annual total precipitation on wet days (PRCP-TOT). Table 1 shows the indices of teleconnections used in this study. More details about these indices are available on the website <https://www.esrl.noaa.gov/psd/data/climateindices/list>, of the National Centers for Environmental Prediction (NCEP).

## 2.3 Behavior of the teleconnections

### 2.3.1 Pearson correlation coefficient

The Pearson method was applied to analyze the behavior of the teleconnections and their influence on the annual precipitation for the studied region. The population correlation coefficient (parameter)  $\rho$  and its sample estimate are closely related to the normal bivariate distribution, whose probability density function is given by:

$$f_{X,Y}(X, Y) = \frac{1}{2\pi\sigma_X\sigma_Y\sqrt{1-\rho^2}} \exp\left\{-\frac{1}{2(1-\rho^2)}\left[\left(\frac{X-\mu_X}{\sigma_X}\right) - 2\rho\left(\frac{Y-\mu_Y}{\sigma_Y}\right) + \left(\frac{Y-\mu_Y}{\sigma_Y}\right)^2\right]\right\} \quad (1)$$

where,  $\rho = \rho_{X,Y} = \frac{COV(X, Y)}{\sigma_X\sigma_Y} = \frac{\sigma_{X,Y}}{\sigma_X\sigma_Y}$  is the population parameter in which  $COV(X, Y)$  is the covariance between  $X$  and  $Y$ ,  $\sigma_X$  is the standard deviation of  $X$ , and  $\sigma_Y$  is the standard deviation of  $Y$ . The Maximum Likelihood Estimator is given by the expression:

$$\hat{\rho}_{X,Y} = \hat{\rho} = \frac{\sum_{i=1}^n (X_i - \bar{X})(Y_i - \bar{Y})}{n\sqrt{\sum_{i=1}^n \frac{(X_i - \bar{X})^2}{n}} \sqrt{\sum_{i=1}^n \frac{(Y_i - \bar{Y})^2}{n}}} = \frac{\sum_{i=1}^n (X_i - \bar{X})(Y_i - \bar{Y})}{n\hat{\sigma}_X\hat{\sigma}_Y} \quad (2)$$

where  $n$  is the number of observations of the sample,  $\bar{X}$  is the arithmetic mean of  $X$ , and  $\bar{Y}$  is the arithmetic mean of  $Y$ . The correlation coefficient,  $\rho$ , can also be interpreted in terms of  $\rho^2$ , which is known as the coefficient of determination. When multiplied by 100,  $\rho^2$  yields the percentage of the variation in the dependent variable  $Y$  that can be explained by the variation in the independent variable  $X$ . In other words, it quantifies the proportion of the variance in  $Y$  that is predictable from  $X$ , that is, how much variation is

shared by both variables. The coefficient of determination is the ratio of the variance explained by the linear regression model ( $Y = \alpha + \beta X$ , where  $\alpha$  and  $\beta$  are constants) to the total variance in  $Y$ .

The significance of the estimated correlation coefficient is verified through hypothesis testing. The statistic to test the hypothesis  $H_0: \rho = 0$  against  $H_1: \rho \neq 0$  has distribution  $t$  with  $n - 2$  degrees of freedom, that is:

$$t = \frac{\hat{\rho}\sqrt{n-2}}{\sqrt{1-\hat{\rho}^2}} \sim t_{n-2} \quad (3)$$

In this work, the correlation analysis between the precipitation series of the 113 GPCC grids with the four distinct teleconnections was performed, and the values were spatialized over the entire NEB. In addition, it is worth noting that different significance levels between the obtained correlations were tested, and the results with confidence levels greater than 0.01 were highlighted.

### 2.3.2 Rainfall Anomaly Index (RAI)

In this work, the RAI was used to analyze precipitation on a monthly, seasonal, and annual scales and address droughts that affect agriculture, water resources, and other sectors (Kraus 1977). This index considers the classification of precipitation values to calculate positive and negative precipitation anomalies and was chosen because it is flexible in the precipitation analysis. The following equation defines such an index:

$$RAI_{\text{positive}} = 3 \left[ \frac{(N - N_1)}{(M - N_1)} \right], \quad \text{and} \quad RAI_{\text{negative}} = -3 \left[ \frac{(N - N_1)}{(X - N_1)} \right], \quad (4)$$

where  $N$  is the annual precipitation for a given year,  $N_1$  is the average annual precipitation of the historical series,  $M$  is the average of the ten most extensive historical precipitation time series, and  $X$  is the average of the ten shortest historical precipitation time series. In this work, RAI series were calculated based on the average rainfall of the entire NEB and the four mesoregions. In addition, to categorize the RAI values into different severity classes, the rainfall classification defined by Van-Rooij (1965) was used, as shown in Table 2.

**Table 2** Rainfall classification according to RAI

RAI	Classification	RAI	Classification
$\geq 3.00$	Extremely wet	$-0.99$ to $-0.50$	Slightly dry
2.00 to 2.99	Very wet	$-1.99$ to $-1.00$	Moderately dry
1.00 to 1.99	Moderately wet	$-2.99$ to $-2.00$	Very dry
0.50 to 0.99	Slightly wet	$\leq -3.00$	Extremely dry
0.49 to $-0.49$	Near normal		

### 2.3.3 Cross-wavelet analysis

In this study, we employed cross-wavelet analysis to examine the coherence between the selected teleconnection indices and precipitation, as represented by the RAI, across different timescales. The combination of cross-wavelet analysis and RAI allowed us to identify the periods during which the teleconnections and precipitation were significantly related, as well as the timescales of their interactions. By analyzing these relationships, we were able to better understand the influence of atmospheric teleconnections on precipitation variability in NEB and provide a more comprehensive assessment of the underlying climatic processes. Cross-wavelet analysis shows the covariance of energy between two time series and reveals information about the relationship between their phases. As in Fourier transform analysis, the wavelet power spectrum can be extended to analyze two time series,  $X_n$  and  $Y_n$  (Grinsted et al. 2004). Considering

the continuous form, it is possible to define the Continuous Wavelet Transform of these two series as  $WXY = WXWY^*$ , where the asterisk denotes the conjugate complex; furthermore, we define the wavelet cross power spectrum as  $|W^{XY}|$ . The theoretical distribution of the cross-spectrum background energy of the wavelets of two time series  $P_K^X$  and  $P_K^Y$  is defined in Torrence and Compo (1998) as:

$$D\left(\frac{|W_n^X(s)W_n^{Y*}(s)|}{\sigma_X\sigma_Y} < p\right) = \frac{Z_v(p)}{v} \sqrt{P_k^X P_k^Y} \tag{5}$$

Equation (5) shows the theoretical distribution of the cross-wavelet transform power spectrum over two time series (Torrence and Compo 1998). Thus,  $Z_v(p)$  is the confidence level associated with probability  $p$ , for a Probability Density Function, defined by the square root of the product of two  $\chi^2$  (Chi-square). In this paper, cross-wavelet analyses were performed considering the RAI series of each of the four

**Fig. 2** Variation of annual average precipitation in the mesoregions and NEB (1901–2013)

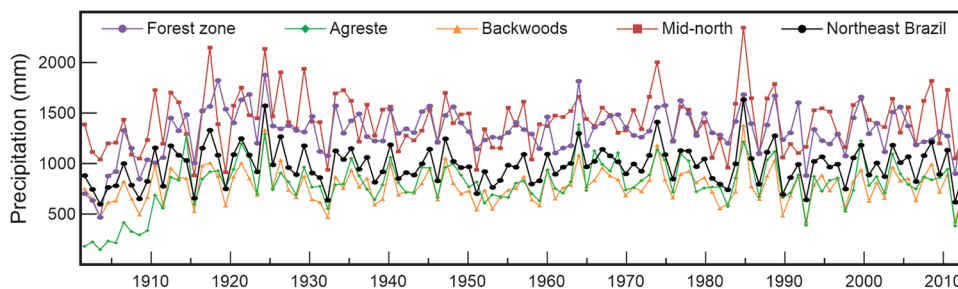
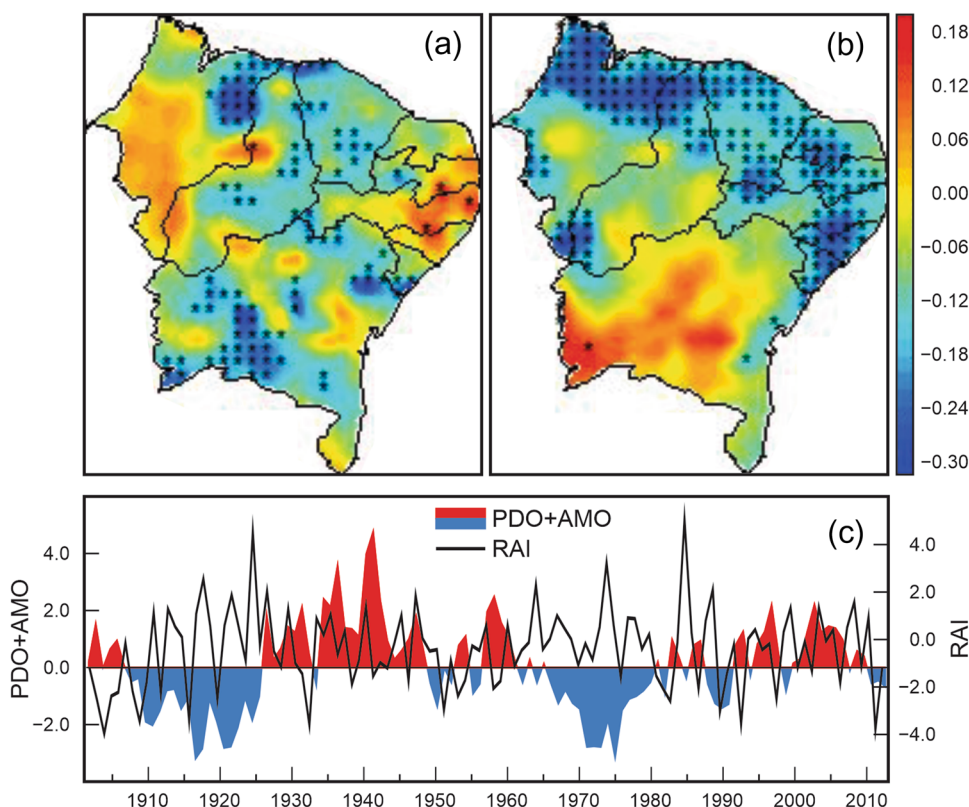


**Fig. 3** Correlation between PRCPTOT (mm) and **a** AMO and **b** PDO, where dotted areas correspond to correlations showing statistical significance at the 0.1 level, and **c** time series of normalized PDO+AMO, 1901–2013



regions with the series of the four teleconnections. In this sense, 16 coherence analyses were developed between these signals, highlighting the robustness of the work developed.

### 3 Results

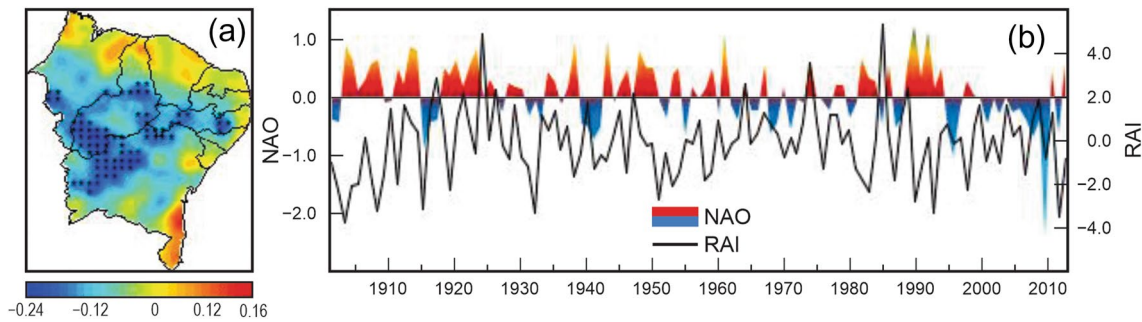
#### 3.1 Correlation between the PRCPTOT and atmospheric teleconnections

Figure 2 shows the variation of annual average precipitation in the mesoregions and NEB from 1901 to 2013. Upon analyzing this figure, it is evident that the highest precipitation values are concentrated in the Mid-north and Forest zone mesoregions, respectively, with rainfall exceeding 2000 and 1400 mm/year. The Backwoods and Agreste mesoregions exhibit the lowest precipitation values, with rainfall ranging between 500 and 900 mm/year.

Figure 3a, b show the correlation between PRCPTOT and AMO and PDO, respectively, while Fig. 3c shows the time series of the normalized PDO + AMO from 1901 to 2013. The relationship between PRCPTOT and AMO for the 1901

to 2013 period shows significant negative correlation coefficients in the northern, central, and southern parts (Fig. 3a). The multidecadal variability in NEB presents a more powerful influence in the Backwoods than the continental influence on precipitation.

On the other hand, the PDO shows a significant negative correlation in the northern, eastern, and western sectors of NEB, indicating an inverse pattern of precipitation with the PDO (Fig. 3b). During the warm phase of the PDO, precipitation in NEB is below average, and the cold phase results in wetter conditions. The normalized PDO + AMO shows a cooling between 1901–1924 and 1949–1989 and warming between 1926 and 1946 and from 1990 onwards (Fig. 3c). These results indicate that PDO + AMO influences the climate in NEB. The warm PDO mode is associated with more frequent El Niños, and the warm AMO mode on an annual basis correlates with generalized warming. Thus, when the PDO and AMO are in their warm modes, one can expect more warmth, while when both are in their cold modes, one expects climate cooling over the region.



**Fig. 4** **a** Spatial distribution of the correlation of PRCPTOT (mm) with NAO, and **b** time series of NAO and PRCPTOT, period 1901 to 2013. The dotted areas correspond to correlations showing statistical significance at the 0.1 level corresponding to correlation coefficients

of  $\pm 0.184 \leq r < \pm 0.156$ ; the 0.05 significance level corresponds to values of  $\pm 0.185 \leq r < \pm 0.241$  and the 0.01 significance level corresponds to  $r \geq \pm 0.242$

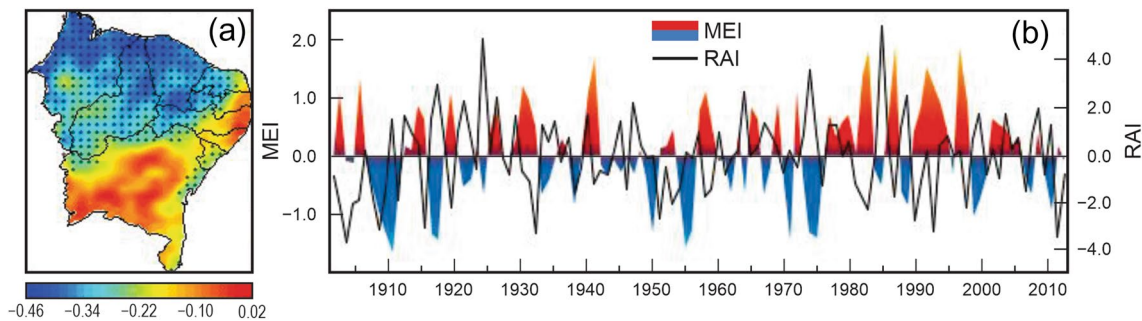


**Fig. 5** **a** Spatial distribution of the correlation of PRCPTOT (mm) and MEI, and **b** time series of MEI and PRCPTOT, period 1901 to 2013. The dotted areas correspond to correlations that show statistical significance at the 0.1 level, corresponding to correlation coefficients

of  $\pm 0.184 \leq r < \pm 0.156$ ; the 0.05 significance level corresponds to values of  $\pm 0.185 \leq r < \pm 0.241$ , and the 0.01 significance level corresponds to  $r \geq \pm 0.242$

The NAO has two pressure systems that affect the direction of the westerly winds, i.e., the low-pressure system located in Iceland and the high-pressure system in the Azores. During the 1901–2013 period, the NAO shows significant negative correlation coefficients in the central-western sector of NEB (Fig. 4a). The positive phase of the NAO corresponds to the intensification of high-altitude westerly winds, which arrive with greater speed at subpolar latitudes and guide storms across the Atlantic between Newfoundland and Northern Europe (Wallace and Gutzler 1981). The NAO was in a predominantly positive phase at the beginning of the twentieth century, while the negative phase was more pronounced between the 1940s and 1970s (Weisheimer et al. 2017). Hurrell (1995) states that the positive and negative phases of the NAO are strongly associated with the location and intensity of the jet stream and, as a consequence, with the trajectory of depressions in the North Atlantic. Figure 4b shows the variability of RAI during the different phases of the MEI. It can be seen that NAO and RAI show high variability and that NAO remains at the same stage for some years. On the other hand, during the positive phase of the NAO, the climatic conditions in NEB become more conducive to the occurrence of drought episodes (Fig. 4b).

The MEI and precipitation show negative correlation coefficients, indicating opposite characteristics of SST and bearing geographic variations in their seasonal characteristics (Fig. 5a). Negative MEI values represent the cold ENSO phase (La Niña), while positive MEI values represent the warm ENSO phase (El Niño). In the years from 1901 to 2013, La Niña of strong intensity occurred in the years: (1903–1904, 1906–1908, 1909–1910, 1916–1918, 1938–1939, 1949–1951, 1954–1956, 1973–1976, 1988–1989, and 2007–2008); and El Niño of strong intensity in the years: (1902–1903, 1905–1906, 1911–1912, 1918–1919, 1925–1926, 1939–1941, 1957–1959, 1972–1973, 1982–1983, 1990–1993, and 1997–1998). El Niño events of greatest amplitude occurred in 1982–1983 and 1997–1998, presenting major climate impacts over the period studied, 1901 to 2013.

### 3.2 Cross-wavelet analysis of RAI and atmospheric teleconnections

The following results show the periodicity of the RAI with AMO, PDO, NAO, and MEI through cross-wavelet analysis. Figure 6 shows that AMO and RAI present periodicity on the 30-year scale. This result is more noticeable in the Forest zone in the 1930–1980 period, Agreste in 1930–1990, and

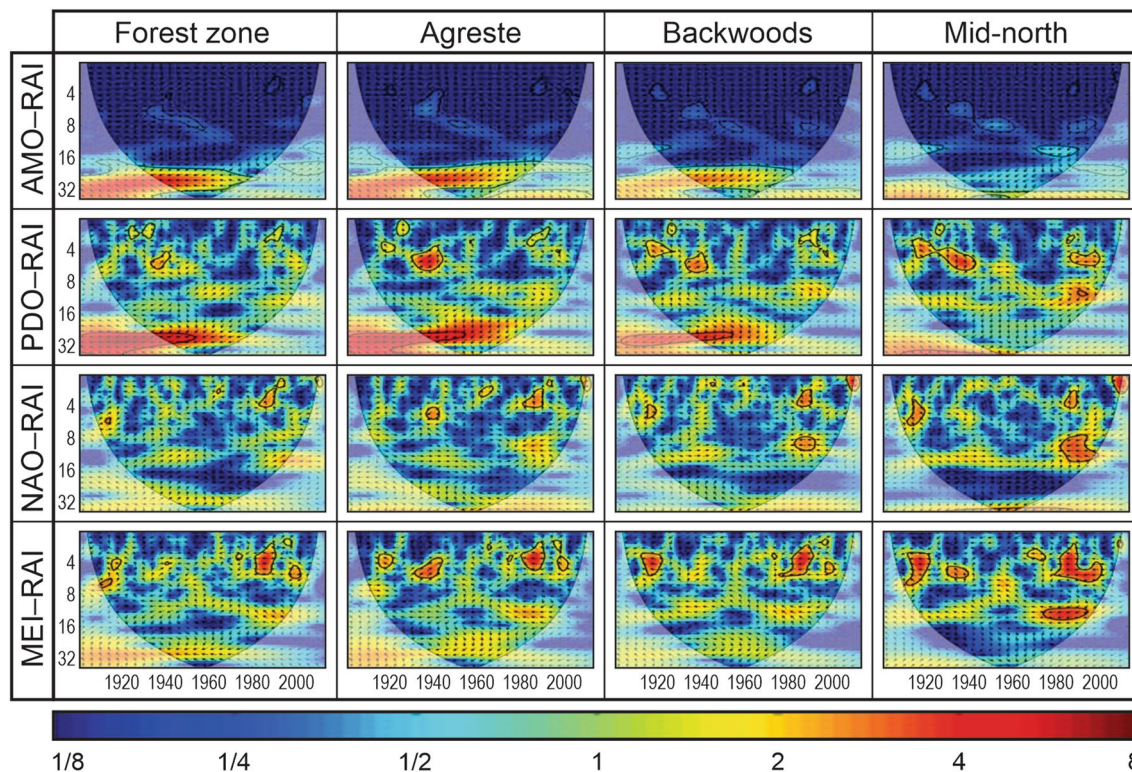


**Fig. 6** Cross-wavelet transform of the standardized AMO and RAI time series (upper pane) and cross-wavelet transform of the standardized MEI and RAI time series (lower pane). The relative phase relationship is shown as arrows (with in-phase pointing right, anti-phase

pointing left, and RAI leading oscillation by 90° pointing straight down). The lighter region is the cone of influence, where zero padding has reduced the variance. The 5% significance level against red noise is shown as a thick contour



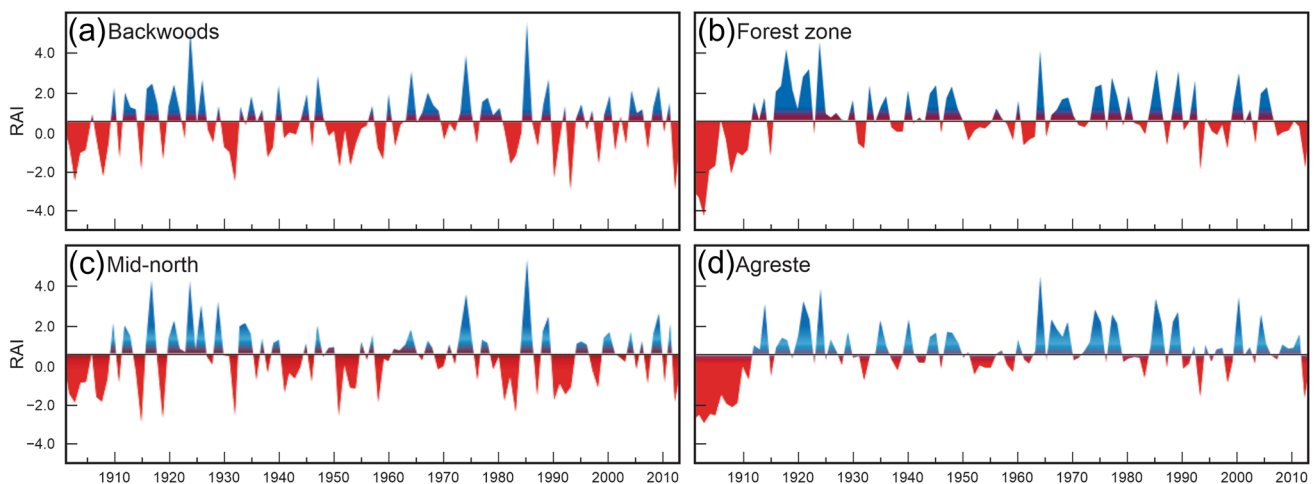


**Fig. 7** RAI variability in the four NEB mesoregions

Backwoods in 1930–1980, while the phase vectors between AMO and RAI are in opposite phases. On the other hand, in the Mid-north, the periodicity of 32 years was observed during the 1940–1965 period. The PDO and RAI present interannual periodicities at different scales and in all mesoregions. There is a 30-year interdecadal periodicity in the Forest zone, Agreste, and Backwoods in 1935–1950, with phase vectors indicating that RAI is advanced  $135^\circ$  from PDO, i.e., PDO accounts for  $3/8$  of the period (11.25 years). In the Mid-north, a periodicity of approximately 6 years is observed in 1915–1945, with the RAI lagging  $225^\circ$  from the PDO, i.e., the RAI responds to  $3/8$  of the period (2.25 years), and in 1985–2000, with the RAI and PDO in opposite phases.

### 3.3 Variability of the RAI in NEB mesoregions

Figure 7 shows the variability of the RAI in the four NEB mesoregions. In the Backwoods, the years 1903, 1908, 1932, 1990, 1993, and 2012 were considered extremely dry, coinciding with strong intensity El Niño episodes in 1903 and weak intensity in 1993, while the years 1924, 1974, and 1985 were considered extremely wet, coinciding with moderate intensity La Niña episodes in 1924 and 1974. In the Forest zone, the years 1901–1903 were extremely dry, coinciding with El Niño episodes of strong intensity. The years 1918, 1924, and 1964, on the other hand, were considered extremely humid, coinciding with the occurrence of La Niña of moderate intensity.

## 4 Discussion

### 4.1 Correlation between the PRCPTOT index and atmospheric teleconnections

Phase transitions from one mode to the other are abrupt and occur within a year or two (Intergovernmental Panel

on Climate Change—Fourth Assessment Report AR4), which makes these oscillations related to oceanic patterns or thermohaline circulation (D'Aleo and Taylor 2007). Cool AMO phases occurred in the 1900–1920 and 1960–1980 periods, while a warm phase occurred in the 1930–1950 period. These periods coincide with examples of anomalous regional climate: for example, 1930–1950 showed decreased rainfall in NEB, reduced river flows in the United States, enhanced Sahel rainfall, and hurricane formation. Conversely, 1960–1980 was a period of high rainfall in NEB, and high river flows in the US, while Sahel rainfall and Atlantic hurricane formation were reduced (Knight et al. 2006). Knight et al. (2006) showed that the positive phase of the AMO is associated with a northward shift of the ITCZ over the Tropical Atlantic, together with a northward equatorial crosswind anomaly. The study further points out that in the twentieth century, periods of high precipitation in NEB coincided with the negative phase of the AMO (1900–1920 and 1960–1980), while the positive phase (1930–1950) coincided with below-average precipitation.

According to Andreoli and Kayano (2007), the precipitation anomalies in NEB can be attributed primarily to the action of the anomalous Walker circulation, adjusted through the rearrangement of convection in the eastern equatorial Pacific. During El Niño years, the displacement of the Walker circulation hinders the formation of clouds and reduces rainfall during the rainy season. During El Niño episodes, positive precipitation anomalies occur in typically arid and semiarid regions, such as the west coast of South America, the southern United States, and East Africa (Anyamba 2001; Holmgren et al. 2006).

Furthermore, the El Niño phenomenon, which is characterized by anomalous warming of the surface waters in the central and eastern equatorial Pacific, is a key factor influencing the occurrence of drought in the semiarid region

of Brazil. These studies help to better understand the influence of El Niño on hydroclimatic variability in the region, particularly in the semiarid region of Brazil located in sub-regions Backwoods and Agreste that are particularly vulnerable to the impacts of El Niño due to their already arid climate and limited water resources. The reduced rainfall during drought periods can lead to water scarcity, crop failure, and food insecurity, affecting both rural and urban populations. The results of this study corroborate those obtained by other researchers who have analyzed historical data on ocean temperatures and precipitation patterns (Hernández Ayala 2019; King et al. 2023). These studies have shown that El Niño events are associated with a decrease in rainfall in northeastern Brazil, particularly in its semiarid region. Overall, the El Niño phenomenon plays a significant role in shaping the hydroclimate of the semiarid region of Brazil, with important impacts on the livelihoods and well-being of local communities.

However, recent studies suggest the existence of several El Niño types. For example, the eastern Pacific coast experienced stronger impacts from the 1997–1998 ENSO than those expected from the 2015–2016 ENSO, despite having similar tropical SST anomalies (Capotondi et al. 2015; Jacox et al. 2016; Tovar et al. 2018). The understanding of El Niño–Southern Oscillation (ENSO) teleconnections in the extratropics is based on the paradigms of tropical and subtropical responses to thermal forcing in the tropical Pacific (Gill 1980; Sardeshmukh and Hoskins 1988) and the propagation of resulting Rossby waves into the extratropics (King et al. 2023). Understanding the spatiotemporal variability of annual, monthly, and seasonal rainfall is crucial for determining the risk of droughts, soil erosion, floods, and developing soil conservation plans (Musabbir et al. 2023).

#### 4.2 Cross-wavelet analysis of RAI and atmospheric teleconnections

The NAO and the RAI present interannual periodicity at different scales, with greater predominance in the Mid-north mesoregion. In the Forest zone, the MEI and the RAI present periodicity of 4–6 years in 1980–1990, with the MEI and RAI in opposite phases; in the Agreste, a periodicity of 4 years is observed in three distinct periods: in 1915–1920, with the RAI responding to 1.5 years of the period; in 1930–1945, with the RAI lagged 45° of the MEI, that is, the RAI responds to 6 months of the period; and in 1980–1990, with the MEI and RAI in opposite phases. In the Backwoods, the MEI and RAI show a periodicity of 4 years in 1915–1925 and 1980–1990, with the MEI and RAI in opposite phases; in the Mid-north, a periodicity of 4–6 years is observed in 1915–1925, 1930–1940, 1970–1975, and

1985–2005, and periodicity of 15 years in 1975–1995, with the MEI and RAI in opposite phases.

#### 4.3 Variability of the RAI in NEB mesoregions

In the Mid-north, the years 1915, 1919, 1932, 1951, and 1983 were extremely dry and coincided with the occurrence of El Niño episodes of moderate intensity (1915 and 1951) and strong intensity (1919 and 1983). The years 1917, 1924, 1974, and 1985 were considered extremely wet, with La Niña episodes of strong (1917), moderate (1924), and weak (1974) intensities. In the Agreste, the 1901–1905 period was considered extremely dry and coincided with strong (1902–1903) and moderate (1904–1905) El Niño intensity. The years 1924, 1964, 1985, and 2000 were considerably wet, with moderate La Niña events in 1924 and 2000.

The Backwoods and Mid-north are the regions most susceptible to climatic fluctuations and drought episodes. For the 1901–1913 period and according to the RAI, 47 drought episodes were identified in the Backwoods and 45 drought episodes in the Mid-north. In the Agreste, 30 drought episodes were identified, and in the Forest zone, 36 episodes of drought. According to Lee et al. (2023), the El Niño/Southern Oscillation (ENSO) is a combined phenomenon of fluctuating sea surface temperature and atmospheric circulation over the central and eastern Pacific Ocean. It has a critical influence on climate patterns all over the world. During the El Niño events, the monthly rainfall anomalies are below normal.

### 5 Conclusions

In this research, the influence of different atmospheric teleconnections on the total annual precipitation of NEB for the 1901–2013 period, considering the physical characteristics of subregions Mid-north, Backwoods, Agreste, and Forest zone, was analyzed. The results obtained showed that different indices of teleconnections can be used to understand the influence of global scale teleconnections on precipitation in NEB. In addition, the statistical techniques of cross wavelet and RAI, coupled with oceanic and atmospheric patterns, indicated changes in the climatic indices of the Pacific Ocean and the Atlantic Ocean, as well as climatic variability and the influence of external forces in the evolution of NEB climate patterns.

The results show differences in the modulation of the atmospheric teleconnections in the sub-regions of NEB. The AMO modulates precipitation in NEB in the four sub-regions on an interannual scale, with greater influence in the Backwoods. Still, the PDO exerts greater control over the modulation of weather patterns in NEB. In the

Agreste and Forest zone, the PDO impacts precipitation on an interannual- and decadal-scale, and in the Mid-north and Backwoods, on an interannual scale in discontinuous periods. It is also pointed out that external and anthropogenic forcings affect the local convection, interfering with the Atlantic and Pacific oceanic conditions.

The MEI shows greater variability in the Mid-north mesoregion, indicating the intensification of La Niña phenomena in the northwestern sector of NEB on an interannual scale and on different time scales. The NAO impacts the RAI on an interannual- and decadal-scale in the Mid-north and on an interannual scale in the Backwoods, Agreste, and Forest zone.

**Acknowledgements** This work was funded by the Foundation for Research Support of the State of Paraíba. The authors are grateful to NCEP/NCAR for the teleconnections data, which are publicly available from <https://www.esrl.noaa.gov/psd/data/climateindices/list/> and precipitation data <https://www.esrl.noaa.gov/psd/data/gridded/data.gpcp.html>.

**Author contributions** DCS: conceptualization, methodology, data curation, writing—original draft preparation. CAGS: conceptualization, methodology, visualization, writing—original draft preparation, writing—reviewing and editing. RMBN: writing—reviewing and editing. RMS: visualization, writing—reviewing and editing. CACS: writing—reviewing and editing.

**Funding** This study was financed in part by the National Council for Scientific and Technological Development, Brazil (313358/2021-4, 309330/2021-1, 420031/2021-9, and 409800/2022-8), the Brazilian Agency for the Improvement of Higher Education (Coordenação de Aperfeiçoamento de Pessoal de Nível Superior—CAPES)—Fund Code 001, and the Federal University of Paraíba (Public call No. 01/2021 Produtividade em Pesquisa PROPESQ/PRPG/UFPB proposal code: PVF14853-2021).

**Data availability** Data will be made available on reasonable request.

## Declarations

**Conflict of interest** On behalf of all authors, the corresponding author states that there is no conflict of interest.

**Open Access** This article is licensed under a Creative Commons Attribution 4.0 International License, which permits use, sharing, adaptation, distribution and reproduction in any medium or format, as long as you give appropriate credit to the original author(s) and the source, provide a link to the Creative Commons licence, and indicate if changes were made. The images or other third party material in this article are included in the article's Creative Commons licence, unless indicated otherwise in a credit line to the material. If material is not included in the article's Creative Commons licence and your intended use is not permitted by statutory regulation or exceeds the permitted use, you will need to obtain permission directly from the copyright holder. To view a copy of this licence, visit <http://creativecommons.org/licenses/by/4.0/>.

## References

Alizamir M, Shiri J, Fard AF, Kim S, Docheshmeh Gorgij A, Heddam S, Singh VP (2023) Improving the accuracy of daily solar

- radiation prediction by climatic data using an efficient hybrid deep learning model: Long short-term memory (LSTM) network coupled with wavelet transform. *Eng Appl Artif Intell* 123(1):106199. <https://doi.org/10.1016/j.engappai.2023.106199>
- Andrade MC (1980) *A Terra e o homem no Nordeste*, 4th edn. Livraria Editora Ciências Humana, São Paulo
- Andreoli RV, Kayano MT (2007) A importância relativa do Atlântico Tropical Sul e Pacífico Leste na variabilidade da precipitação do Nordeste do Brasil. *Rev Bras Meteorol* 22(1):63–74. <https://doi.org/10.1590/S0102-77862007000100007>
- Anyamba A (2001) NDVI anomaly patterns over Africa during the 1997/98 ENSO warm event. *Int J Remote Sens* 22(10):1847–1859. <https://doi.org/10.1080/01431160010029156>
- Araghi A, Mousavi-Baygi M, Adamowski J, Martinez C (2016) Association between three prominent climatic teleconnections and precipitation in Iran using wavelet coherence. *Int J Climatol* 37(6):2809–2830. <https://doi.org/10.1002/joc.4881>
- Basheer M, Elagib NA (2016) Performance of satellite-based and GPCP 7.0 rainfall products in an extremely data-scarce country in the Nile Basin. *Atmos Res* 215:128–140. <https://doi.org/10.1016/j.atmosres.2018.08.028>
- Brasil Neto RM, Santos CAG, Nascimento TVM, Silva RM, Santos CAC (2020) Evaluation of the TRMM product for monitoring drought over Paraíba State, northeastern Brazil: a statistical analysis. *Remote Sens* 12:2184. <https://doi.org/10.3390/rs12142184>
- Brasil Neto RM, Santos CAG, Silva RM, Santos CAC (2022) Evaluation of TRMM satellite dataset for monitoring meteorological drought in north-eastern Brazil. *Hydrol Sci J* 67(14):1119–1135. <https://doi.org/10.1080/02626667.2022.2130333>
- Brito CS, Silva RM, Santos CAG, Brasil Neto RM, Coelho VHR (2021) Monitoring meteorological drought in a semiarid region using two long-term satellite-estimated rainfall datasets: A case study of the Piranhas River basin, northeastern Brazil. *Atmos Res* 250:105380. <https://doi.org/10.1016/j.atmosres.2020.105380>
- Cabré A, Marinov I, Gnanadesikan A (2017) Global atmospheric teleconnections and multidecadal climate oscillations driven by Southern Ocean convection. *J Clim* 30(20):8107–8126. <https://doi.org/10.1175/jcli-d-16-0741.1>
- Capotondi A, Wittenberg AT, Newman M, Di Lorenzo E, Yu JY, Brannon P, Cole J, Boris D, Giese B, Guilyardi E, Jin FF, Karnauskas K, Kirtman B, Lee T, Schneider N, Xue Y, Yeh SW (2015) Understanding ENSO diversity. *Bull Am Meteorol Soc* 96(6):921–938. <https://doi.org/10.1175/bams-d-13-00117.1>
- Chang X, Wang B, Yan Y, Hao Y, Zhang M (2018) Characterizing effects of monsoons and climate teleconnections on precipitation in China using wavelet coherence and global coherence. *Clim Dyn* 51(327):1–16. <https://doi.org/10.1007/s00382-018-4439-1>
- Chiang JCH, Friedman AR (2012) Extratropical cooling, interhemispheric thermal gradients, and tropical climate change. *Annu Rev Earth Planet Sci* 40(1):383–412. <https://doi.org/10.1146/annurev-earth-042711-105545>
- Chiang JCH, Kushnir Y, Giannini A (2002) Deconstructing Atlantic Intertropical Convergence Zone variability: influence of the local cross-equatorial sea surface temperature gradient and remote forcing from the eastern equatorial Pacific. *J Geophys* 107(D1):3–19. <https://doi.org/10.1029/2000JD000307>
- Costa DD, Uvo CB, Paz AR, Carvalho FO, Fragoso CR Jr (2018) Long-term relationships between climate oscillation and basin-scale hydrological variability during rainy season in eastern Northeast Brazil. *Hydrol Sci J* 63(11):1636–1652. <https://doi.org/10.1080/02626667.2018.1523614>
- D'Aleo J, Taylor G (2007) Temperature cycles in North America, Greenland and the Arctic, relationship to multidecadal ocean cycles and solar trends. <http://ruby.fgcu.edu/courses/twimberley/EnviroPhilo/TempCyclesUS.pdf>. Accessed 26 June 2017

- Da Silva GS, Amarante PA, Amarante JCA (2022) Agricultural clusters and poverty in municipalities in the Northeast Region of Brazil: a spatial perspective. *J Rural Studies* 92:189–205. <https://doi.org/10.1016/j.jrurstud.2022.03.024>
- Dantas JC, Silva RM, Santos CAG (2020) Drought impacts, social organization and public policies in northeastern Brazil: a case study of the Upper Paraíba River basin. *Environ Monit Assess* 192:317. <https://doi.org/10.1007/s10661-020-8219-0>
- Delazeri LMM, Da Cunha DA, Oliveira LR (2022) Climate change and rural–urban migration in the Brazilian Northeast region. *GeoJournal* 87:2159–2179. <https://doi.org/10.1007/s10708-020-10349-3>
- Dufek AS, Ambrizzi T (2008) Precipitation variability in São Paulo State, Brazil. *Theor Appl Climatol* 93(3–4):167–178. <https://doi.org/10.1007/s00704-007-0348-7>
- Fan W, Hu Z, Ma W, Ma Y, Yang Y, Yu H, Han X (2022) Impacts of mid-high latitude atmospheric teleconnection patterns on interannual variation of the Tibetan Plateau summer monsoon. *Atmos Res* 275:106219. <https://doi.org/10.1016/j.atmosres.2022.106219>
- Giannini A, Saravanan R, Chang P (2004) The preconditioning role of Tropical Atlantic variability in the prediction of Nordeste rainfall during ENSO events. *Clim Dyn* 22(8):839–855. <https://doi.org/10.1007/s00382-004-0420-2>
- Gill AE (1980) Some simple solutions for heat-induced tropical circulations. *Q J R Meteorol Soc* 106:447–462. <https://doi.org/10.1002/qj.49710644905>
- Grimm AM, Saboia JPI (2015) Interdecadal variability of the South American precipitation in the monsoon season. *J Clim* 28(2):755–775. <https://doi.org/10.1175/JCLI-D-14-00046.1>
- Grinsted A, Moore JC, Jevrejeva S (2004) Application of the cross wavelet transform and wavelet coherence to geophysical time series. *Nonlinear Process Geophys* 11:561–566. <https://doi.org/10.5194/npg-11-561-2004>
- Han L, Long J, Xu F, Xu J (2022) Decadal shift in sea fog frequency over the northern South China Sea in spring: Interdecadal variation and impact of the Pacific Decadal Oscillation. *Atmos Res* 265:105905. <https://doi.org/10.1016/j.atmosres.2021.105905>
- Hastenrath S, Lamb P (1977) *Climatic Atlas of the Tropical Atlantic and Eastern Pacific Oceans*. University of Wisconsin Press, Madison
- Hernández Ayala JJ (2019) Atmospheric teleconnections and their effects on the annual and seasonal rainfall climatology of Puerto Rico. *Theor Appl Climatol* 137:2915–2925. <https://doi.org/10.1007/s00704-019-02774-3>
- Holmgren M, Stapp J, Dickman CR, Gracia C, Graham S, Gutiérrez JR, Hice C, Jaksic F, Kelt DA, Letnic M, Lima M, López BC, Meserve PL, Milstead WB, Polis GA, Previtali MA, Richter M, Sabaté S, Squeo FA (2006) Extreme climatic events shape arid and semiarid ecosystems. *Front Ecol Environ* 4(2):87–95. [https://doi.org/10.1890/1540-9295\(2006\)004\[0087:ECESAA\]2.0.CO;2](https://doi.org/10.1890/1540-9295(2006)004[0087:ECESAA]2.0.CO;2)
- Huo X, Lei L, Liu Z, Hao Y, Hu BX, Zhan H (2016) Application of wavelet coherence method to investigate Karst Spring discharge response to climate teleconnection patterns. *J Am Water Resour Assoc* 52(6):1281–1296. <https://doi.org/10.1111/1752-1688.12452>
- Hurrell JW (1995) Decadal trends in the North Atlantic Oscillation regional temperatures and precipitation. *Science* 269(5224):676–679. [https://doi.org/10.1126/science.269.5224.676#\\_blank](https://doi.org/10.1126/science.269.5224.676#_blank)
- IBGE—Instituto Brasileiro de Geografia e Estatística (2010) *Censo Demográfico 2010. Resultados gerais da amostra*. IBGE, Rio de Janeiro
- Jacox MG, Hazen EL, Zaba KD, Rudnick DL, Edwards CA, Moore AM, Bograd SJ (2016) Impacts of the 2015–2016 El Niño on the California Current System: early assessment and comparison to past events. *Geophys Res Lett* 43(13):7072–7080. <https://doi.org/10.1002/2016gl069716>
- Jemai S, Ellouze M, Abida H (2017) Variability of precipitation in arid climates using the wavelet approach: case study of watershed of Gabes in South-East Tunisia. *Atmosphere* 8(9):178. <https://doi.org/10.3390/atmos8090178>
- Kayano MT, Andreoli RV (2009) *Clima da Região Nordeste do Brasil*. In: Cavalcanti, IFA (org.) *Tempo e Clima no Brasil*, Oficina de Textos, pp 213–218
- King MP, Keenlyside N, Li C (2023) ENSO teleconnections in terms of non-NAO and NAO atmospheric variability. *Clim Dyn*. <https://doi.org/10.1007/s00382-023-06697-8>
- Knight JR, Folland CK, Scaife AA (2006) Climate impacts of the Atlantic multidecadal oscillation. *Geophys Res Lett* 33(17):L17706. <https://doi.org/10.1029/2006GL026242>
- Kraus EB (1977) Subtropical droughts and cross-equatorial energy transports. *Mon Weather Rev* 105(8):1009–1018. [https://doi.org/10.1175/15200493\(1977\)105%3c1009:sdacee%3e2.0.co;2](https://doi.org/10.1175/15200493(1977)105%3c1009:sdacee%3e2.0.co;2)
- Kundzewicz ZW, Hirabayashi Y, Kanae S (2010) River floods in the changing climate—observations and projections. *Water Resour Manag* 24(11):2633–2646. <https://doi.org/10.1007/s11269-009-9571-6>
- Lau NC (2015) Bernhard Haurwitz Memorial Lecture: model diagnosis of El Niño teleconnections to the global atmosphere–ocean system. *Bull Am Meteorol Soc* 97(6):981–988. <https://doi.org/10.1175/bams-d-15-00220.1>
- Lee JH, Julien PY, Cho J, Lee S, Kim J, Kang W (2023) Rainfall erosivity variability over the United States associated with large-scale climate variations by El Niño/southern oscillation. *CATENA* 226:107050. <https://doi.org/10.1016/j.catena.2023.107050>
- Leng G, Tang Q, Rayburg S (2015) Climate change impacts on meteorological, agricultural and hydrological droughts in China. *Global Planet Change* 126:23–34. <https://doi.org/10.1016/j.gloplacha.2015.01.003>
- Lim YK, Schubert SD, Chang Y, Molod AM, Pawson S (2018) The impact of SST-forced and unforced teleconnections on 2015/16 El Niño winter precipitation over the Western United States. *J Clim* 31(15):5825–5844. <https://doi.org/10.1175/jcli-d-17-0218.1>
- Molavi-Arabshahi M, Arpe K, Leroy SAG (2015) Precipitation and temperature of the southwest Caspian Sea region during the last 55 years: their trends and teleconnections with large-scale atmospheric phenomena. *Int J Climatol* 36(5):2156–2172. <https://doi.org/10.1002/joc.4483>
- Moreira E, Targino I, Rodrigues MF (2007) Manuel Correia de Andrade: uma vida de trabalho em defesa de uma ciência geográfica socialmente comprometida. *OKARA Geografia Em Debate* 1(1):143–145
- Musabbir M, Islam ARMT, Rahman MS, Pal SC, Alam E, Mallick J (2023) Spatiotemporal variability of rainfall erosivity and its teleconnection with atmospheric circulation in monsoon-driven climate region. *CATENA* 221(Part A):106762. <https://doi.org/10.1016/j.catena.2022.106762>
- Nascimento TVM, Santos CAG, Farias CAS, Silva RM (2022) Monthly streamflow modeling based on self-organizing maps and satellite-estimated rainfall data. *Water Resour Manag* 36:2359–2377. <https://doi.org/10.1007/s11269-022-03147-8>
- NCAR—National Center for Atmospheric Research (2019) *NCAR Climate Data Guide Content With Tag: Zhang, Rong*. <https://climatedataguide.ucar.edu/experts/zhang-rong>. Accessed 02 Apr 2019
- NCDC—National Climatic Data Center (2019) *Teleconnections*. <https://www.ncdc.noaa.gov/teleconnections/>. Accessed 02 Apr 2019
- NCSU—North Carolina State University. *Global Patterns*. <https://climate.ncsu.edu/climate/patterns/pdo>. Accessed 02 Apr 2019
- Ndehedehe CE, Anyah RO, Alsdorf D, Agutu NO, Ferreira VG (2018) Modelling the impacts of global multi-scale climatic drivers on hydro-climatic extremes (1901–2014) over the Congo basin. *Sci*






- Total Environ 651:1569–1587. <https://doi.org/10.1016/j.scitotenv.2018.09.203>
- Okumura YM, DiNezio P, Deser C (2017) Evolving impacts of multi-year La Niña events on atmospheric circulation and US drought. *Geophys Res Lett* 44(22):614–623. <https://doi.org/10.1002/2017GL075034>
- Park JH, Li T (2018) Interdecadal modulation of El Niño-tropical North Atlantic teleconnection by the Atlantic multi-decadal oscillation. *Clim Dyn* 52(328):1–16. <https://doi.org/10.1007/s00382-018-4452-4>
- Rao VB, de Brito JIB (1985) Teleconnections between the rainfall over Northeast Brazil and the winter circulation of Northern Hemisphere. *Pure Appl Geophys* 123:951–959. <https://doi.org/10.1007/BF00876982>
- Safanelli JL, Nôia Júnior RS, Coutinho PAQ, de Araujo MA, Fendrich AN, Rizzo R, Chamma ALS, Tavares PA, Barretto AGOP, Maule RF, Reichardt K, Sparovek G, Dourado Neto D (2023) Grain-cropping suitability for evaluating the agricultural land use change in Brazil. *Appl Geogr* 154:102937. <https://doi.org/10.1016/j.apgeog.2023.102937>
- Santos CAG, Freire PKMM, Torrence C (2013) A transformada wavelet e sua aplicação na análise de séries hidrológicas. *Rev Bras Rec Hídricas* 18(3):271–280. <https://doi.org/10.21168/rbrh.v18n3.p271-280>
- Santos CAG, Kisi Ö, Silva RM, Zounemat-Kermani M (2018) Wavelet-based variability on streamflow at 40-year timescale in the Black Sea region of Turkey. *Arab J Geosci* 11:169. <https://doi.org/10.1007/s12517-018-3514-6>
- Santos CAG, Freire PKMM, Silva RM, Akrami AS (2019) Hybrid wavelet neural network approach for daily inflow forecasting using Tropical Rainfall Measuring Mission Data. *J Hydrol Eng* 24:04018062. [https://doi.org/10.1061/\(asce\)he.1943-5584.0001725](https://doi.org/10.1061/(asce)he.1943-5584.0001725)
- Santos CAG, Nascimento GR, Farias CAS, Silva RM, Mishra M (2023) Short- and long-term streamflow forecasting using wavelet neural networks for complex watersheds: a case study in the Mahanadi River, India. *Ecol Inform* 73:101945. <https://doi.org/10.1016/j.ecoinf.2022.101945>
- Sardeshmukh PD, Hoskins BJ (1988) The generation of global rotational flow by steady idealized tropical divergence. *J Atmos Sci* 45:1228–1251. [https://doi.org/10.1175/1520-0469\(1988\)045%3C1228:TGOGRF%3E2.0.CO;2](https://doi.org/10.1175/1520-0469(1988)045%3C1228:TGOGRF%3E2.0.CO;2)
- Schamm K, Ziese M, Becker A, Finger P, Meyer-Christoffer A, Schneider U, Schröder M, Stender P (2014) Global gridded precipitation over land: a description of the new GPCP First Guess Daily product. *Earth Syst Sci Data* 6(1):49–60. <https://doi.org/10.5194/essd-6-49-2014>
- Schneider U, Ziese M, Meyer-Christoffer A, Finger P, Rustemeier E, Becker A (2016) The new portfolio of global precipitation data products of the Global Precipitation Climatology Centre suitable to assess and quantify the global water cycle and resources. *Proc IAHS* 374:29–34. <https://doi.org/10.5194/piahs-374-29-2016>
- Silva BKN, Lucio PS, Silva CMS, Spyrides MHC, Silva MT, Andradre LMB (2017) Characterization agricultural vulnerability to drought in the Northeast of Brazil. *Nat Hazards Earth Syst Sci Discuss*. <https://doi.org/10.5194/nhess-2017-377>
- Silva JS, Silva RM, Santos CAG (2018) Spatiotemporal impact of land use/land cover changes on urban heat islands: a case study of Paço do Lumiar, Brazil. *Build Environ* 136:279–292. <https://doi.org/10.1016/j.buildenv.2018.03.041>
- Silva IM, Medeiros DM, Mesquita MS (2020) Investigating teleconnection patterns associated with the rainy season of the northern northeast Brazil using a hidden Markov model. *Clim Dyn* 55:2075–2088. <https://doi.org/10.1007/s00382-020-05374-4>
- Silva AM, Silva RM, Santos CAG, Linhares FM, Xavier APC (2022) Modeling the effects of future climate and land use changes on streamflow in a headwater basin in the Brazilian Caatinga biome. *Geocarto Int* 37(26):12436–12465. <https://doi.org/10.1080/10106049.2022.2068672>
- Silva Junior CHL, Celentano D, Rousseau GX, de Moura EG, Varga IvD, Martinez C, Martins MB (2020) Amazon forest on the edge of collapse in the Maranhão State, Brazil. *Land Use Policy* 97:104806. <https://doi.org/10.1016/j.landusepol.2020.104806>
- Stan C, Straus DM, Frederiksen JS, Lin H, Maloney ED, Schumacher C (2017) Review of tropical-extratropical teleconnections on intraseasonal time scales. *Rev Geophys* 55(4):902–937. <https://doi.org/10.1002/2016rg000538>
- Su L, Miao C, Borthwick A, Duan Q (2017) Wavelet-based variability of Yellow River discharge at 500-, 100-, and 50-year timescales. *Gondwana Res* 49(9):94–105. <https://doi.org/10.1016/j.gr.2017.05.013>
- Surendran U, Anagha B, Gopinath G, Joseph EJ (2019) Long-term rainfall analysis towards detection of meteorological drought over Kozhikode district of Kerala. *J Clim Change* 5(2):23–34. <https://doi.org/10.3233/jcc190010>
- Thornton PK, Ericksen PJ, Herrero M, Challinor AJ (2014) Climate variability and vulnerability to climate change: a review. *Global Change Biol* 20(11):3313–3328. <https://doi.org/10.1111/gcb.12581>
- Torrence C, Compo GP (1998) A practical guide to wavelet analysis. *Bull Am Meteorol Soc* 79(1):61–78. [https://doi.org/10.1175/15200477\(1998\)079%3c0061:APGTWA%3e2.0.CO;2](https://doi.org/10.1175/15200477(1998)079%3c0061:APGTWA%3e2.0.CO;2)
- Tovar C, Infantas ES, Roth VT (2018) Plant community dynamics of lomas fog oasis of Central Peru after the extreme precipitation caused by the 1997–98 El Niño event. *PLoS One* 13(1):1–19. <https://doi.org/10.1371/journal.pone.0190572>
- Van-Rooy MP (1965) A Rainfall Anomaly Index (RAI). Independent of the time and space. *Notas* 14:43–48
- Verdon DC, Wyatt AM, Kiem AS, Franks SW (2004) Multidecadal variability of rainfall and streamflow: Eastern Australia. *Water Resour Res* 40(10):W10201. <https://doi.org/10.1029/2004WR003234>
- Vining BR, Hillman A, Contreras DA (2022) El Niño Southern Oscillation and enhanced arid land vegetation productivity in NW South America. *J Arid Environ* 198:104695. <https://doi.org/10.1016/j.jaridenv.2021.104695>
- Wallace JM, Gutzler DS (1981) Teleconnections in the Geopotential Height Field during the Northern Hemisphere Winter. *Mon Weather Rev* 109(4):784–812. [https://doi.org/10.1175/1520-0493\(1981\)109%3c0784:TITGHF%3e2.0.CO;2](https://doi.org/10.1175/1520-0493(1981)109%3c0784:TITGHF%3e2.0.CO;2)
- Wang Z, Yang S, Lau NC, Duan A (2018) Teleconnection between summer NAO and East China rainfall variations: a bridge effect of the Tibetan Plateau. *J Clim* 31:6433–6444. <https://doi.org/10.1175/JCLI-D-17-0413.1>
- Weisheimer A, Schaller N, O'reilly C, Macleod DA, Palmer T (2017) Atmospheric seasonal forecasts of the twentieth century: multi-decadal variability in predictive skill of the winter North Atlantic Oscillation (NAO) and their potential value for extreme event attribution. *Q J R Meteorol Soc* 143(703):917–926. <https://doi.org/10.1002/qj.2976>
- Xiao M, Zhang Q, Singh VP (2016) Spatiotemporal variations of extreme precipitation regimes during 1961–2010 and possible teleconnections with climate indices across China. *Int J Climatol* 37(1):468–479. <https://doi.org/10.1002/joc.4719>
- Zhao Z, Lin Z, Li F, Rogers BM (2022) Influence of atmospheric teleconnections on interannual variability of Arctic-boreal fires. *Sci Total Environ* 838(Part 4):156550. <https://doi.org/10.1016/j.scitotenv.2022.156550>
- Zhou F, Zhao Z, Azorin-Molina C, Jia X, Zhang G, Chen D, Liu J, Guijarro JA, Zhang F, Fang K (2022) Teleconnections between large-scale oceanic-atmospheric patterns and interannual surface wind speed variability across China: Regional and seasonal patterns.

Sci Total Environ 838(1):156023. <https://doi.org/10.1016/j.scitotenv.2022.156023>

Zin WZW, Jamaludin S, Deni SM, Jemain AA (2010) Recent changes in extreme rainfall events in Peninsular Malaysia: 1971–2005. *Theor Appl Climatol* 99(3):303–314. <https://doi.org/10.1007/s00704-009-0141-x>

**Publisher's Note** Springer Nature remains neutral with regard to jurisdictional claims in published maps and institutional affiliations.

## Authors and Affiliations

Daris Correia dos Santos<sup>1</sup>  · Celso Augusto Guimarães Santos<sup>1</sup>  · Reginaldo Moura Brasil Neto<sup>1</sup>  ·  
Richarde Marques da Silva<sup>2</sup>  · Carlos Antonio Costa dos Santos<sup>3</sup> 

✉ Celso Augusto Guimarães Santos  
celso@ct.ufpb.br

<sup>1</sup> Department of Civil and Environmental Engineering,  
Federal University of Paraíba, João Pessoa 58051-900,  
Brazil

<sup>2</sup> Department of Geosciences, Federal University of Paraíba,  
João Pessoa 58051-900, Brazil

<sup>3</sup> Graduate Program in Meteorology, Federal University  
of Campina Grande, Campina Grande 58109-970, Brazil